Journal of System Design and Dynamics

Vol. 4, No. 1, 2010

Design and Development of Electric Active Stabilizer Suspension System*

Shuuichi BUMA**, Yasuhiro OOKUMA**, Akiya TANEDA***,
Katsumi SUZUKI***, Jae-Sung CHO**** and Masaru KOBAYASHI*****

**1, Toyota-Cho, Toyota, Aichi, 471-8572 Japan
E-mail: s@buma.tec.toyota.co.jp
***Aisin Seiki Co., Ltd.
2-1, Asahi-machi, Kariya, Aichi, 448-8650 Japan
****Toyota Technical Development Corporation
1-21, Imae, Hanamoto-Cho, Toyota, Aichi, 470-0334 Japan
*****Harmonic Drive Systems Inc.
1856-1 Maaki, Hotaka-Machi, Minamiazumi-Gun, Nagano, 399-8305 Japan

Abstract

An electric active stabilizer suspension system has been developed as a technology for controlling vehicle roll. The system includes various sensors that detect the vehicle's running state, and active stabilizer actuators that use electric motors and reduction gears to control roll. The electric stabilizer suspension system was compared with hydraulic stabilizer systems, and an investigation demonstrated the superiority of the developed system, which offers outstanding vehicle behavior, improved responsiveness and reduced energy consumption (including energy regeneration).

Key words: Motion Control, Actuator, Maneuverability/Vehicle Dynamics, Suspension System, Active

1. Introduction

The world's first active suspension system for improving ride comfort and vehicle stability was developed in Japan in 1989 and subsequently adopted in various models [(1)-(3)]. However, due to its large mass and energy consumption, use of this system ceased in the second half of the 1990s as more economical vehicles gained popularity. However, an active stabilizer control system was developed in Europe in 2002 that applied control in the roll direction only [(4)]. Subsequently, in 2005, the authors developed an active stabilizer suspension system utilizing the reverse efficiency of reduction gears and electric motor control to reduce energy consumption to 1/20 of a conventional system [(5)-(9)]. Figure 1 shows the structure of this active stabilizer suspension system.

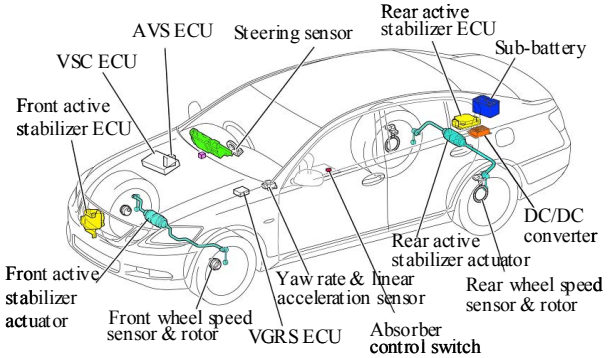

Fig.1 Arrangement of system components

*Received 1 Sep., 2009 (No. T1-08-7019)
Japanese Original : Trans. Jpn. Soc. Mech. Eng., Vol.74, No.748, C (2008), pp.2827-2836 (Received 30 May, 2008)
[DOI: 10.1299/jsdd.4.61]

This paper describes the design of the active stabilizer suspension system, focusing on the required actuator performance that was set based on real-world use conditions and reduction gear reverse efficiency. It also describes operational simulations of the system and the results of actual vehicle evaluations.

2. Electric Actuator Design

2.1 Required Actuator Performance

2.1.1 Computational Formula for Actuator Torque

Figure 2 shows the vehicle specifications that determine the longitudinal and lateral distribution of tire vertical reaction force due to the lateral acceleration generated when cornering, which acts on the center of gravity of the vehicle body [10].

Figure 3 shows the front view model for calculating the amount of variation in tire vertical load at each wheel. The model depicts the vertical load variation ΔW_f as divided between the tire position coil spring reaction force f_{cf} and the stabilizer actuator reaction force f_{tf}. This diagram shows the case of the front suspension, and the suffix "*f*" should be changed to "*r*" to represent the rear suspension.

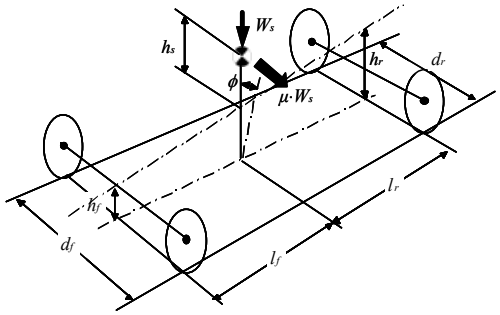

Fig.2 Schematic drawing of vehicle lateral force and dimensions

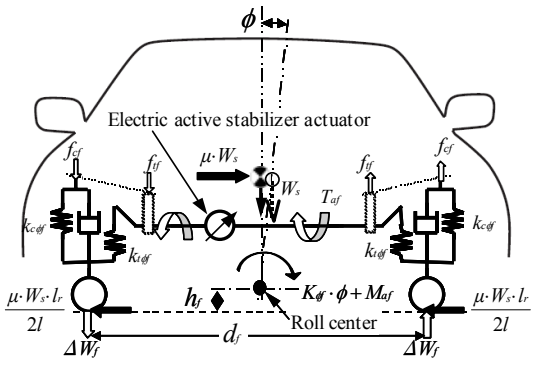

Fig.3 Vertical load variation of vehicle roll

The active stabilizer suspension system supports roll moment caused by lateral acceleration when cornering using the roll reaction force obtained from the roll stiffness of the suspension and the roll reaction force of the electric actuators. Equation (1) expresses the moment equilibrium around the sprung roll center. The left side of the equation shows the sum of the roll reaction force of the suspension roll stiffness and the roll moment M_{af} and M_{ar} generated by the electric actuators. Equation (2) shows the case of the front wheels in detail.

$$\left(K_{\phi f} + K_{\phi r}\right) \cdot \phi + M_{af} + M_{ar} = \mu \cdot W_s \cdot h_s + W_s \cdot h_s \cdot \phi \tag{1}$$

$$K_{\phi f} \cdot \phi + M_{af} = 2K_{c\phi f} \cdot \phi + 2K_{t\phi f} \cdot \phi + M_{af} \tag{2}$$

$K_{c\,\phi f}\cdot\phi$ on the right side of the equation shows the single wheel coil spring roll moment. $K_{t\,\phi f}\cdot\phi$ is the single wheel passive roll moment generated by the torsion springs of the electric actuators, and M_{af} is the active roll moment generated by the electric actuators.

The spring and the motor of the electric actuator are arranged in series. Thus, $K_{t\,\phi f}\cdot\phi + M_{af}$ in Eq. (2) shows that, within the range of the actuator reduction gear reverse efficiency, the torsion spring twists in reaction to the roll angle, which increases the return torque of the electric actuator even when the motor torque remains constant. Equation (3) shows the distribution of M_{af} and M_{ar} in Eq. (1) by the roll stiffness ratio α. The electric actuator active roll moment M_{af} can be calculated by Eq. (4) from Eqs. (1) and (2).

$$M_{ar} = \frac{(1-\alpha)}{\alpha}\cdot M_{af} \tag{3}$$

$$M_{af} = \alpha\cdot\left[\mu\cdot W_S\cdot h_S - \phi\cdot\left(K_{\phi f} + K_{\phi r} - W_S\cdot h_S\right)\right] \tag{4}$$

Equation (5) expresses the moment equilibrium around the unsprung roll center.

$$K_{\phi f}\cdot\phi + M_{af} = \Delta W_f\cdot d_f - \frac{\mu\cdot W_S\cdot l_r}{l}\cdot h_f \tag{5}$$

The vertical load variation ΔW_f at the tire can be obtained from Eq. (5) and is shown as Eq. (6). In the same way, ΔW_r can be shown as Eq. (7).

$$\Delta W_f = \frac{\left(K_{\phi f}\cdot\phi + M_{af}\right)}{d_f} + \frac{\mu\cdot W_S\cdot l_r}{d_f\cdot l}\cdot h_f \tag{6}$$

$$\Delta Wr = \frac{\left(K_{\phi r}\cdot\phi + M_{ar}\right)}{d_r} + \frac{\mu\cdot W_S\cdot l_f}{d_r\cdot l}\cdot h_r \tag{7}$$

The vertical load variations obtained from these equations can be re-distributed as desired vertical load distributions β (0.5 to 0.7) based on the dynamic performance of the vehicle. This is shown in Eqs. (8) and (9).

$$\Delta W'_f = \beta\cdot\left(\Delta W_f + \Delta Wr\right) \tag{8}$$

$$\Delta W'r = \left(1-\beta\right)\cdot\left(\Delta W_f + \Delta Wr\right) \tag{9}$$

The electric actuator active torque M'_{af} and M'_{ar} can be calculated using Eqs. (10) and (11) based on the re-distributed vertical load distributions.

$$M'_{af} = \Delta W'_f\cdot d_f - \frac{\mu\cdot W_S\cdot l_r}{l}\cdot h_f - K_{\phi f}\cdot\phi \tag{10}$$

$$M'_{ar} = \Delta W'_r\cdot d_r - \frac{\mu\cdot W_S\cdot l_f}{l}\cdot h_r - K_{\phi r}\cdot\phi \tag{11}$$

The active torque m_{af} and m_{ar} for the actuator positions in the active stabilizer suspension system can be obtained by conversion using Eqs. (12) and (13). γ_f and γ_r show the arm displacement ratio for positioning the suspension.

$$m_{af} = \gamma_f\cdot M'_{af} \tag{12}$$

$$m_{ar} = \gamma_r\cdot M'_{ar} \tag{13}$$

The equations after converting the torque of the coil springs, electric actuator torsion springs, and electrical portions into actuator positions with respect to the overall roll moment are shown below in the case of the front wheels.

The total roll moment m_{tf} including the coil portions is shown in Eq. (14).

Torque T_{af}, which is the sum of the passive torque of the electric actuator torsion springs and the active torque of the electrical portions is shown in Eq. (15).

$$m_{tf} = \gamma_f \cdot \left(2 \cdot k_{c_{\phi f}} \cdot \phi + 2 \cdot k_{t_{\phi f}} \cdot \phi + M'_{af}\right) \tag{14}$$

$$T_{af} = \gamma_f \cdot \left(2 \cdot k_{t_{\phi f}} \cdot \phi + M'_{af}\right) \tag{15}$$

The proportional distribution of electric actuator active torque m_{af} can be clarified from Eqs. (14) and (15). Table 1 lists the definitions of the symbols and typical values of the calculation formulae.

Table 1 List of symbols and actual values

	Explanation	Actual value (Unit)
Ws	Sprung mass	1762 (Kg)
φ	Vehicle roll angle	0.01745(rad) at5m/s²
hs	Length between roll axis and center of gravity	0.452 (m)
μ	Lateral acceleration	(m/s²)
l	Wheel base	l=2.85 (m)
lf	Front share of wheel base	lf=1.304 (m)
lr	Rear share of wheel base	lr=1.546 (m)
df	Front tread	df=1.536 (m)
dr	Rear tread	dr=1.546 (m)
hf	Front roll center height	hf=0.084 (m)
hr	Rear roll center height	hr=0.09035(m)
Wsf	Front sprung mass	Wsf=956 (Kg)
Wsr	Rear sprung mass	Wsf=806 (Kg)
Maf, (Mar)	Front active roll moment (rear)	(Nm)
γ_f	Front transmission ratio	0.301
γ_r	Front transmission ratio	0.195
maf, (mar)	Front actuator active torqe (rear)	(Nm)
Taf, (Tar)	Front actuator torqe (rear)	(Nm)
ΔWf, (ΔWr)	Front vertical load variation (rear)	(N)
Kφf	Front roll stiffness	Kφf=48380 (Nm/rad)
Kφr	Rear roll stiffness	Kφr=44330(Nm/rad)
α	Front roll stiffness ratio	0.52
kcφf, (kcφr)	Front coil spring rate (rear)	kcφf=10440 (Nm/rad)
ktφf, (ktφr)	Front torsion spring rate (rear)	ktφf=14760 (Nm/rad)
	Suffix $_f$ and $_r$ mean front and rear respectively	

2.1.2 Target Roll Characteristics for Lateral Acceleration

a. Target Roll Angle

The roll angle was used as an evaluation index in the development of a vehicle equipped with the active suspension. Based on the results of roll attitude angle and a subjective evaluation, a target roll angle of 1 degree for a lateral acceleration of 5 m/s^2 was set [(2)]. Figure 4 shows the lateral acceleration and target roll angle posture.

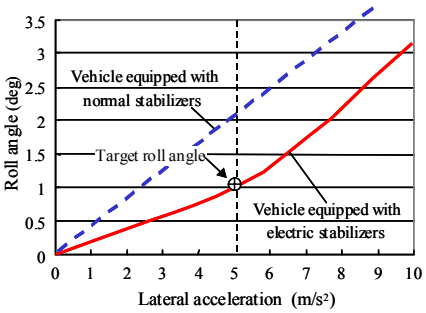

Fig.4 Target roll angle

b. Control Range

Using results from a 167 km driving course including ordinary roads, mountain roads in Hakone, highways, and urban streets, lateral acceleration frequency data equivalent to 200,000 km of real-world driving was accumulated (Fig. 5). Since the maximum lateral acceleration was 5.5 m/s^2, the control range of the electric active stabilizers was set to 5.5 m/s^2 or less (with a gradual change between 5.0 and 5.5 m/s^2). As shown in Fig. 4, the target roll angle for lateral acceleration above this value was set in accordance with the changes in roll angle of normal stabilizers.

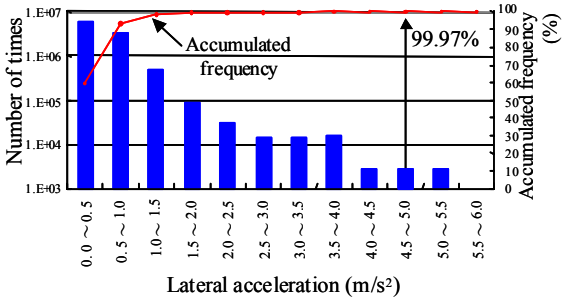

Fig.5 Operation frequency of lateral acceleration

2.1.3 Standard and Reverse Efficiency of Reduction Gear

Compact strain wave gearing to allow a high gear value was adopted. Figure 6 shows the standard efficiency η_p and reverse efficiency η_n of the gear value $1/n$ (1/200).

This graph shows the standard efficiency (during deceleration) below the line of 100% efficiency and the reverse efficiency (during acceleration) above the line. When the motor input torque is 5 Nm, 100% efficiency is defined as an actuator output torque of 1,000 Nm as a result of the magnification by the gear value. These standard and reverse efficiency characteristics were utilized to reduce both the size and energy consumption of the motor.

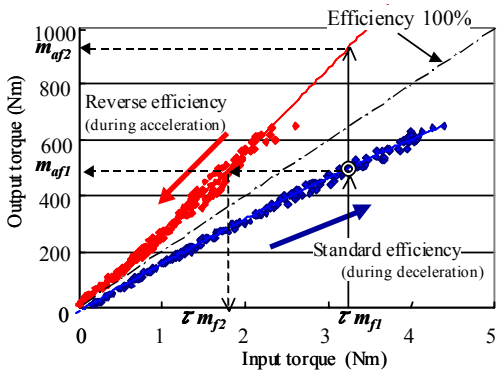

Fig.6 Gear efficiency

a. Increase in Holding Torque

By maintaining the input torque τm_{f1} (i.e., a constant current), the holding torque can be maximized on the actuator return side (m_{af1} to m_{af2}). Equation (16) shows the relationship between the motor input torque τ_{mf1} and actuator active torque m_{af1}. Equation (17) shows the return side holding torque m_{af2}.

$$m_{af1} = \eta_p \cdot n \cdot \tau m_{f1} \tag{16}$$

$$m_{af2} = \frac{1}{\eta_p \cdot \eta_n} \cdot m_{af1} \tag{17}$$

The actually adopted efficiency values for the front electric actuators are η_p: 0.73 and η_n: 0.51. The magnification of return side holding torque is m_{af2}/m_{af1}=2.69, and the maximum torque of the actuators can be obtained up to 2.69 times the torque generated by the motors and the gears.

b. Current Reduction Logic

The motor input torque (current) is reduced by lowering the input torque (τm_{f1} to τm_{f2}) while holding the output torque. Equation (18) shows the relational expression. It is possible to reduce the motor input torque (current) by 1/2.69.

$$\tau m_{f2} = \eta_p \cdot \eta_n \cdot \tau m_{f1} \tag{18}$$

2.1.4 Electric Actuator Requirement Torque

a. Required Active Torque

The following points have already been detailed above.

1) Determination of the computational formulae for torque from the vehicle specifications.
2) Determination of the target roll angle in accordance with lateral acceleration.
3) Determination of the actuator active torque distribution proportions from the reverse efficiency.

Based on these points, the motor requirement torque is calculated using Eqs. (14), (15), and (12). The notation in these equations is as follows.

m_{tf}: total roll moment
T_{af}: passive torque + active torque (electric)
m_{af}: active torque (electric)

Figure 7 shows a calculation graph for a case where the front wheel β=0.52 (equivalent to roll stiffness distribution).

Since the required active torque peaks at a lateral acceleration of 5 m/s^2, smooth gradual changing characteristics were adopted for beyond that point. Figure 8 shows the characteristics set for each vertical load distribution β.

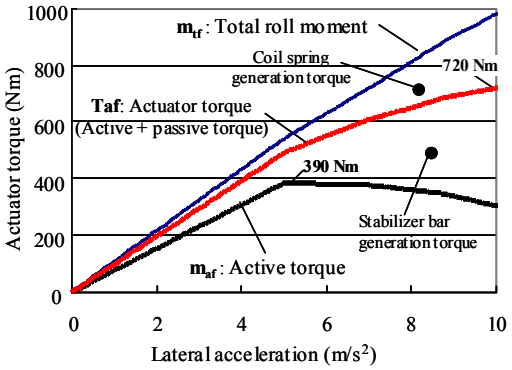

Fig.7 Calculated torque in front rotary actuator (β=0.52)

Considering a vehicle limit lateral acceleration up to 10 m/s^2, the actuator requirement torque is T_{af}=720 Nm.

Equation (19) shows the minimum limit active torque (m_{af}) to obtain this torque (T_{af}).

$$m_{af} \geq \eta_p \cdot \eta_n \cdot T_{af} \tag{19}$$

The maximum active torque m_{af} shown in Fig. 7 is 390 Nm and the value in the right side of Eq. (19) is 720/2.69=268 Nm. Therefore, by establishing Eq. (19), it is possible to set the target roll angle up to an acceleration of 10 m/s^2 within the range of reverse efficiency. Thus, each torque distribution can be determined the same way.

With respect to the required active torque, β=0.7 is used for the maximum vertical load distribution β that contributes to vehicle stability. Accordingly, 585 Nm is set as the required active torque when the lateral acceleration is 5 m/s^2 (shown in Fig. 8).

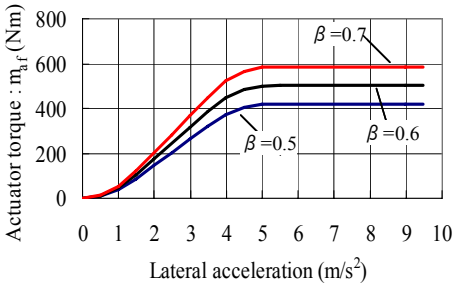

Fig.8 Active torque in front rotary actuator

b. Required Active Torque Rate

After setting the steady state actuator active torque, its response characteristics were determined based on real-world frequency data and vehicle driving conditions. The torque rate is the differential value of the lateral acceleration (i.e., the jerk). Since it has a correlation with the steering angular velocity, the steering angular velocity frequency was investigated on the driving course used to examine the lateral acceleration frequency. Figure 9 shows the results.

The standard steering angular velocity for determining the specifications was set to 150 deg/s, which is a level in excess of twice sigma (σ).

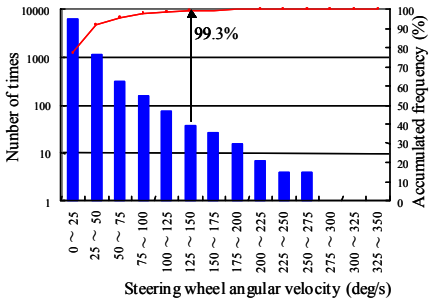

Fig.9 Operation frequency of steering angular velocity

The relationship between the steering angular velocity and lateral acceleration generated in vehicle driving tests was investigated. Figure 10 shows the results.

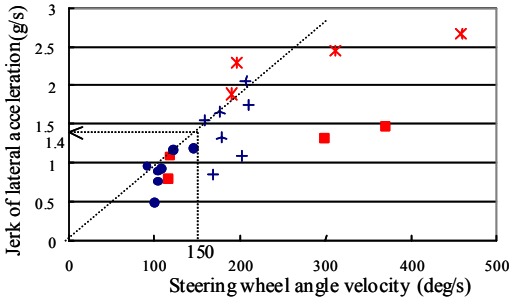

Fig.10 Jerk of lateral acceleration

The driving conditions assumed an object-avoidance situation that requires good vehicle response performance. The vehicle was driven under slalom and lane changing conditions at speeds from 40 km/h to 100 km/h. A steering angular velocity up 150 deg/s was found to represent the majority of real-world driving conditions. Figure 10 shows that 150 deg/s equals a jerk value of 1.4 g/s. Since active torque in normal use (β=0.7) is 501 Nm (at 0.5 g), the required torque rate was set to 1,400 Nm/s.

2.2 Electric Actuator Specifications and Evaluation

2.2.1 Actuator Target Specifications

Table 2 summaries the actuator requirement specifications. Figure 11 shows a sectional view of the main electric actuator body. The electric actuator consists of a motor that supplies the driving force, a reduction gear that amplifies the motor torque, a housing, and a pair of stabilizers.

Table 2 Target specifications (front actuator)

Items		Specification	
Performance	Torque (at 40 A)	Min. 585	(Nm)
	Torque rate (at 17 V)	Min. 1400	(Nm/sec)
	Total stiffness	49	(Nm/deg)
Size	Diameter	Max. 103	(mm)
	Length (main body)	Max. 290	(mm)

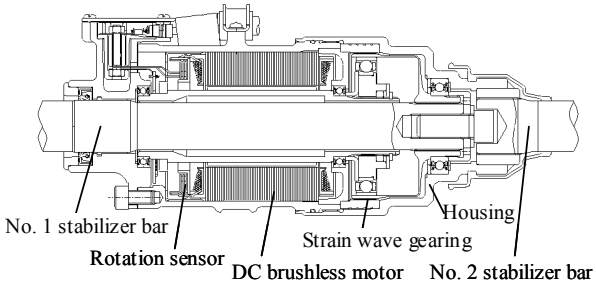

Fig.11 Electric actuator (front)

Motor torque is amplified and transmitted as output torque through the output shaft of the motor, which is connected to the reduction gear, and the output shaft of the reduction gear, which is connected to the No. 1 stabilizer bar. The No. 2 stabilizer bar is fastened to the housing and output torque is transmitted in the opposite direction to the No. 1 stabilizer bar. The electric actuator is also provided with the necessary rotation sensors for controlling the motor. A brushless DC motor is used as the motor to supply the driving force as it enables a hollow structure and has excellent reliability and efficiency.

2.2.2 Basic Structure of Motor

a. Magnet Pole Number and Number of Slots of Motor

The winding specifications of the motor are generally fixed in accordance with the relationship Ns=1.5×p (p: magnet pole number of rotor and Ns: number of slots). The number of slots was studied to reduce the external diameter of the core (stator) as much as possible. As a result, 12 slots and 8 poles were set. Figure 12 shows the relationship between the number of slots and the external diameter of the core.

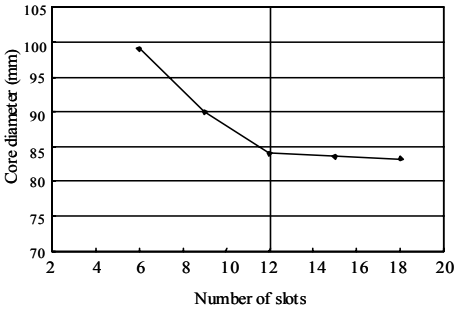

Fig.12 Motor core diameter and number of slots

The adoption of 8 poles instead of 6 poles allows each magnet to be made more compact,

and also reduces the necessary thickness of the hollow shaft. As a result, the moment of inertia was reduced by 23%.

b. Magnet Width

To reduce the vibration of the motor, the angle θ of the magnet width was modified to 32.25 degrees, at which the minimum cogging torque is achieved. Figure 13 shows the relationship between the magnet angle and cogging torque.

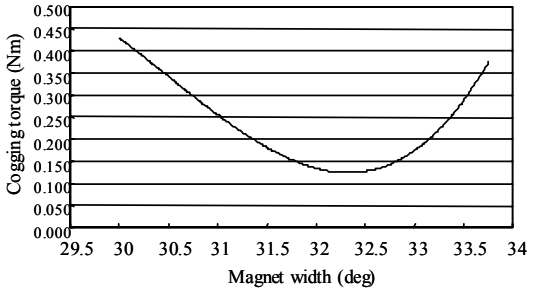

Fig.13 Magnet width and cogging torque

2.2.3 Study of Motor Specifications

Each phase voltage (V_{uv}, V_{vw}, and V_{wu}) and current (I_{uv}, I_{vw}, and I_{wu}) in the motor model is applied in accordance with the following equations to ensure synchronicity with the rotor rotation angle θ.

$$V_{uv} = RI_{uv} + L\frac{d}{dt}(I_{uv}) + E_1 \tag{20}$$

$$V_{vw} = RI_{vw} + L\frac{d}{dt}(I_{vw}) + E_2 \tag{21}$$

$$V_{wu} = RI_{wu} + L\frac{d}{dt}(I_{wu}) + E_3 \tag{22}$$

Where, the counter electromotive force E_1, E_2, and E_3 are obtained as follows.

$$E_1 = K_e\omega\cos(p\theta) \tag{23}$$

$$E_2 = K_e\omega\cos(p\theta - \frac{2}{3}\pi) \tag{24}$$

$$E_3 = K_e\omega\cos(p\theta + \frac{2}{3}\pi) \tag{25}$$

In contrast, the relationship between the motor angular velocity ω and torque τ_m is shown in Eq. (26), and the motor torque is shown in Eq. (27).

$$\tau_m + \tau_o = J\frac{d}{dt}\omega + D\omega \tag{26}$$

$$\tau_m = K_t(I_{uv}\cos(p\theta) + I_{vw}\cos(p\theta - \frac{2}{3}\pi) + I_{wu}\cos(p\theta + \frac{2}{3}\pi)) \quad (27)$$

Where, τ_0 is the load torque, K_e is the counter electromotive force constant, K_t is the torque constant, J is the motor moment of inertia, D is the coefficient of viscosity, R is the resistance, L is the self-inductance, and p is the number of motor pole pairs [11][12]. The actuator specifications are shown in Table 3.

Table 3 Front actuator specifications

Items			Specification	
DC brushless motor	Resistance	R	0.204	(Ω)
	Rotor inertia	J	0.000196	(kgm^2)
	Torque constant	Kt	0.15	(Nm/A)
	Number of pole pairs	p	4	
	Cogging torque		0.1	(Nm)
Electric circuit	External resistance		0.095	(Ω)
	Power supply voltage		17.5	(V)

2.2.4 Bench Evaluation of Electric Actuator

Figure 14 shows the bench test device. The ends of both stabilizer bars were fixed and voltage applied to the motor to test its performance in the standard and reverse rotational directions.

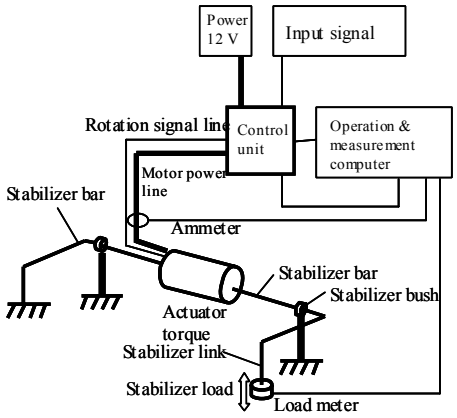

Fig.14 Bench test device

Table 4 shows a typical example of the performance results obtained from the bench evaluation. It was conformed that the actuator achieved the target performance described in Table 2. Figure 15 shows the torque rate in accordance with stepped input of different voltages. The rate at the predetermined voltage of 17 V meets the target value.

Table 4 Bench test result

Items	Result	
Max. torque (at 40 A)	665	(Nm)
Max. torque rate (at 17 V)	1595	(Nm/sec)
Total stiffness	49	(Nm/deg)

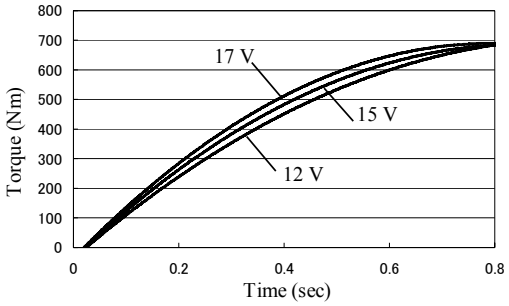

Fig.15 Torque rate at each voltage

Figure 16 shows the frequency response characteristics with sine wave input of torque ±130 Nm. It indicates that the response frequency at a phase lag of 45 degrees is maintained at 2.1 Hz.

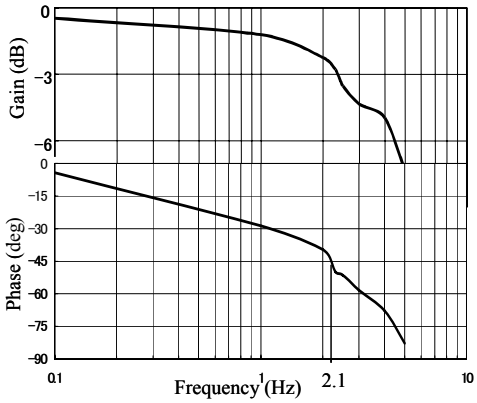

Fig.16 Torque frequency response

3. Simulation

3.1 Simulation Environment

Figure 17 shows the simulation model environment of the active stabilizer suspension system. It consists of a Dymola electric actuator model, a MATLAB/Simulink controller model, and a CarSim vehicle model.

Dymola and CarSim can be simulated on MATLAB/Simulink through a pre-prepared interface (S-Function).

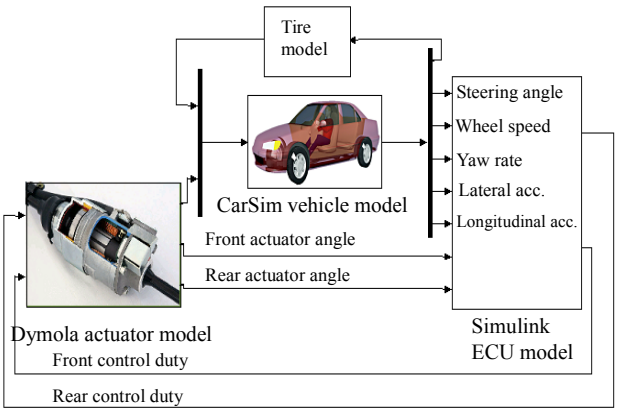

Fig.17 Simulation model environment

3.2 Electric Actuator Model

Figure 18 shows the electric actuator model created using Dymola. Its main components are the stabilizer bars, reduction gear, motor, and drive circuit.

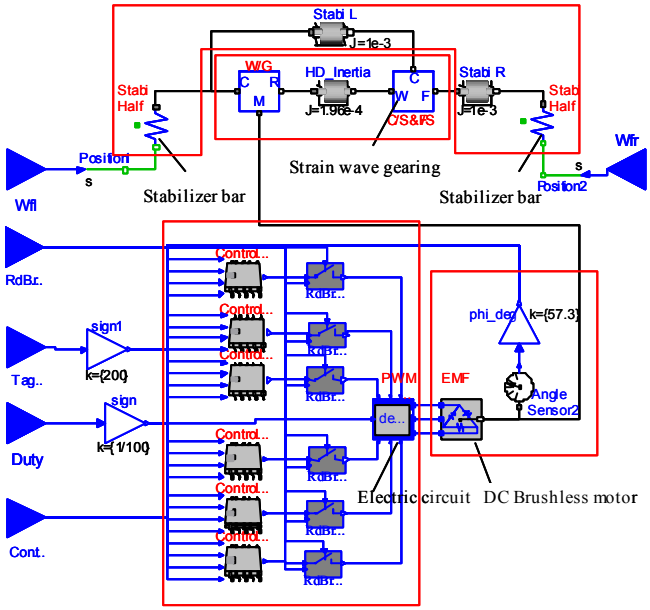

Fig.18 Electric actuator model

3.3 Strain Wave Gearing Model

The reduction gear consists of three elements: a wave generator, flexible splines, and circular splines. The characteristics of the model are as follows.

1) The standard and reverse efficiency properties of the motor are introduced as gear losses.

2) Judgment for standard or reverse input in the model is determined based on whether the product of the torque and rotation speed is positive or negative.

Below, n is the reciprocal of the gear value (200), ω is the rotation speed, τ is the torque, Δ_τ is the torque loss, and τ_b is the loss constant. The suffixes w, f, and c represent the wave generator, flexible splines, and circular splines, respectively. Equations (28) and (29) show the torque transmission.

$$\tau_f = n(\tau_w - \Delta\tau) \tag{28}$$

$$\tau_c = -(n+1)\tau_w + n\Delta\tau \tag{29}$$

Table 5 shows the conditions for determining whether the gear torque transmission has standard or reverse efficiency characteristics. It also shows the torque loss Δ_τ.

Equations (30) and (31) depict the product of ω and τ.

Table 5 Standard and reverse efficiency judgment and torque loss

ω_{wc}	τ_w	$\Delta\tau$
>0	≥ 0	$(1-\eta_p)\cdot\tau_w+\tau_b$
>0	<0	$(1-1/\eta_n)\cdot\tau_w-\tau_b$
<0	≥ 0	$(1-1/\eta_n)\cdot\tau_w-\tau_b$
<0	<0	$(1-\eta_p)\cdot\tau_w+\tau_b$

$$\omega_{wc} \cdot \tau_w \geq 0$$
$$\therefore \Delta\tau = (1-\eta_p) \cdot \tau_w + \tau_b \tag{30}$$

$$\omega_{wc} \cdot \tau_w < 0$$
$$\therefore \Delta\tau = (1-1/\eta_n) \cdot \tau_w - \tau_b \tag{31}$$

Figure 19 shows the standard and reverse efficiency loss using coordinate axes.

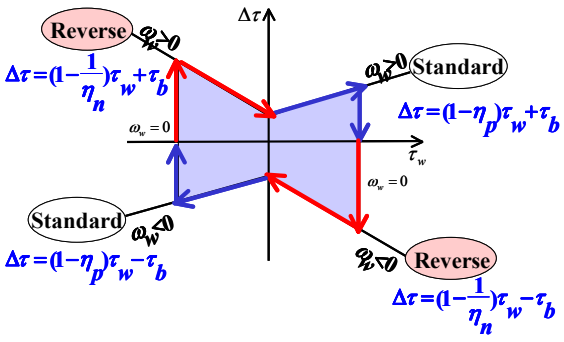

Fig.19 Gear efficiency model

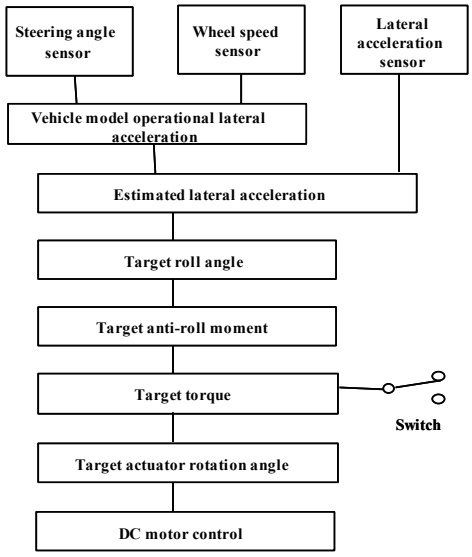

Fig.20 Control logic overview

3.4 Control Specifications

The target actuator rotation angle is controlled based on steering angle signals and a lateral acceleration sensor that are faster than changes in the vehicle roll attitude. Figure 20 shows a block diagram of the control.

3.5 Simulation Results

As part of the system verification, simulations were performed to validate the holding current reduction logic using the key basic standard and reverse efficiency characteristics of

the reduction gears. Figure 21 shows the results of the simulations.

It was confirmed that the power consumption of the system was lowered by actively reducing the applied current when the actual rotation angle of the electric actuator reaches the target rotation angle.

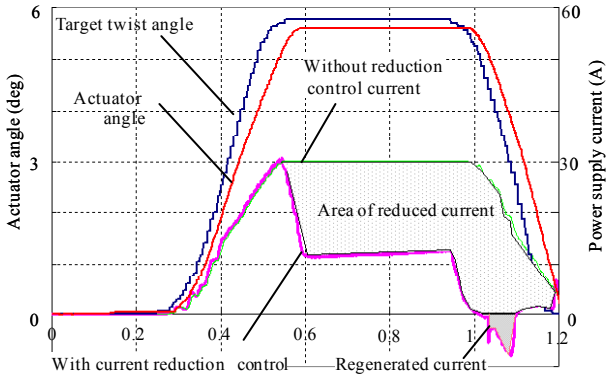

Fig.21 Simulation result of current reduction with the improved control logic

4. Actual Vehicle Evaluation

4.1 Effect of Roll Control

Figure 22 shows the Lissajous curve for the roll angle with respect to lateral acceleration when changing lanes at a speed of 60 km/h. The following results were obtained.

1) The target roll angle of 1 degree at a lateral acceleration of 5 m/s^2 was achieved.

2) The vehicle equipped with the electric stabilizers had a smaller hysteresis width and improved linearity and response than a vehicle equipped with normal stabilizers.

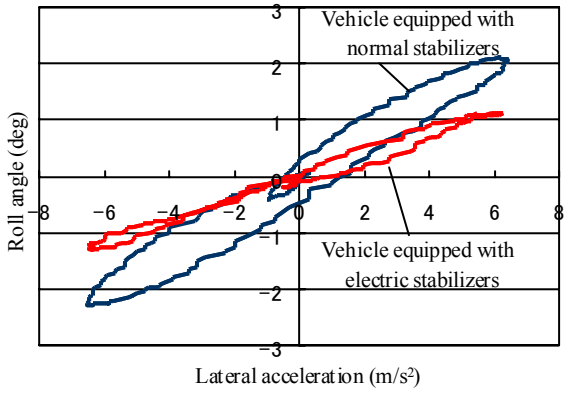

Fig.22 Vehicle roll angles

4.2 Effect of Current Reduction Control

Figure 23 shows the current reduction control with an actual vehicle. Without the current reduction control, once the target rotation angle became constant, a constant current continued to flow. However, with the current reduction control, the current is increased until the actual rotation angle reaches the dead band of the target rotation angle. However, after the target rotation angle becomes constant, the current is reduced when the actual rotation angle reaches the dead band of the target rotation angle, thereby saving energy.

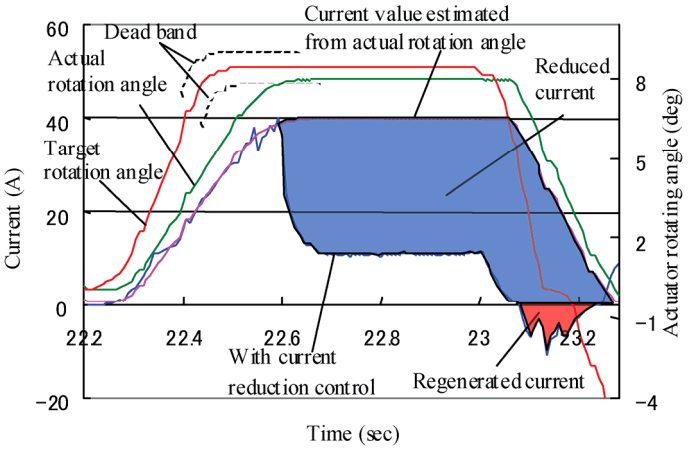

Fig.23 Energy-saving effect of holding current reduction control

The negative portion of the current is regenerated as energy when the actual rotation angle returns due to the stabilizer reaction force. Figure 24 shows the energy consumption of a vehicle equipped with the active stabilizer suspension system on various types of roads. The average value for all roads is 8.8 W.

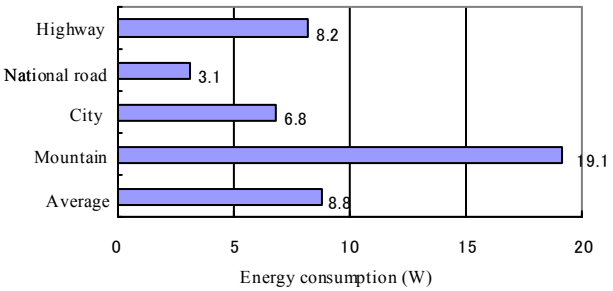

Fig.24 Energy consumption of electric stabilizers

The energy consumption of hydraulic stabilizers with pressure control values that have an equivalent performance as the active stabilizer suspension system (equivalent to the energy consumption of the oil circulation pressure loss when driving in a straight line) is approximately 190 W, which is roughly 22 times that of the active stabilizer suspension system. Therefore, creating an electric system substantially reduces energy consumption.

5. Conclusion

In the development of an active stabilizer suspension system, target performance within a realistic range was determined based on the use environment in the real world. In addition, actuator and system development utilized the reverse efficiency of reduction gears to reduce the size of the electric actuator active torque. The following results were obtained.

1) Setting of specifications based on investigations of real-world use environments

The control range of the system was set to 5.5 m/s^2 based on the frequency of lateral acceleration in the real world. The target roll angle was set to 1 degree (with a lateral acceleration of 5.0 m/s^2) based on prior knowledge of roll feeling [(2)]. For the actuator torque rate, a lateral acceleration jerk of 1.4 g/s was set based on real-world frequency data

for steering angular velocity.

2) Study of effectiveness of gear reverse efficiency characteristics

The electric actuator active requirement torque is a value of at least the sum of the required active and passive torque multiplied by the product of the standard and reverse efficiency. The development identified the usable range of the active requirement torque.

Additionally, the rate capable of holding the return side torque and reducing the input torque was identified using the product of the standard and reverse efficiency. This led to the development of current-reduction logic.

Subsequently, a reduction gear simulation model was used for standard/reverse efficiency judgment, and equations capable of expressing the changes in efficiency as loss were calculated.

As a typical index of vehicle performance, after incorporating the new knowledge obtained in the development into the system, the target roll angle of 1 degree at a lateral acceleration of 5 m/s^2 was achieved. Moreover, average energy consumption was reduced to 8.8 W, which is approximately 1/20 that of a hydraulic system.

References

(1) Yonekawa, T. Ohnuma, T. Mori . Gotoh, T. and Buma, S., Effect of the Active Control Suspension System on Vehicle Dynamics, *JSAE Review*, Vol.12, No.2, pp. 40-45（1991）
(2) Buma, S. Satou,H. Yonekawa, T. Ohnuma, T. Hattori, K. and Sugihara, M., Synthesis and Development of Active Control suspension, *Transactions of the Japan Society of Mechanical Engineers*, *Series C*, Vol. 57, No.534 (1991), pp. 257-263. in Japanese
(3) Akatsu, Y. Iijima. Takahashi. and Murakami., Development of a hydraulic active suspension, *SAE Technical Paper* 931971 (1993)
(4) Dieter Konik., Development of the Dynamic Drive for the new 7 Series of the BMW Group, *International Journal of Vehicle Design*, Vol. 28, No.1/2/3, pp. 131-149（2002）
(5) Buma, S. Urababa, S. Suzuki, S. Ohkuma, Y. Cho, J. and Fukino, T., Electric Active Stabilizer Suspension System, *Journal of the Society of Automotive Engineers of Japan,* Vol. 60**,** NO.**7,** pp. 32-37(2006).
(6) Cho, J. Buma, S. Urababa, S. Ohkuma, Y. Hamada, T. and Kobayashi, Y., Analysis and Development using CAE of the Electric Active Stabilizer Suspension System., *Proceedings. JSAE Annual Congress,* No.11-06, pp. 5-9(2006). in Japanese
(7) Taneda, A. Suzuki, K. Fukino, T. Buma, S. and Urababa, S., Development of the Electric Active Stabilizer Actuator., *Proceedings. JSAE Annual Congress,* No.11-06, pp. 11-15(2006). in Japanese
(8) Ohkuma, Y. Sugimoto, N. Buma, S. Urababa, S. Suzuki, S. Taneda, A. and Kanda, R., Electric Active Stabilizer Suspension System*., Mechanical Engineering Congress, 2006,* Vol.7, pp. 107-108 (2006). in Japanese
(9) Suzuki, K. Taneda, A. Fukino, T. Buma, S. and Kobayashi, Y., Development of the Electric Active Stabilizer Actuator*., Mechanical Engineering Congress, 2006,* Vol.7, pp. 109-110(2006). in Japanese
(10) Abe, M., Vehicle Dymnamics and Control (The 2nd version), *Kabushikikaisya Sankaidou*, p.151-152, in Japanese.
(11) Ferretti,G.,et al., Simulating permanent magnet brushle-ss motors in Dymola, *2nd International Modelica Confernece.* Proceedings,p.109-115.
(12) Hagino, H., Usage of brush-less DC motor, *Ohm sha*, 2003,p.27-34.in Japanese